Unlocking coherent control of ultrafast plasmonic interaction

Eyal Bahar (eyalb@tauex.tau.ac.il)
Tel Aviv University https://orcid.org/0000-0003-1698-6428
Uri Arieli
Tel Aviv University
Maayan Vizner Stern
Tel Aviv University
Suchowski Haim
Tel Aviv University

Article

Keywords: coherent control, ultrafast plasmonic interaction, nonlinear emission

Posted Date: June 23rd, 2021

DOI: https://doi.org/10.21203/rs.3.rs-530232/v1

Unlocking coherent control of ultrafast plasmonic interaction

Authors: Eyal Bahar[1]*, Uri Arieli[1], Maayan Vizner Stern[1], Haim Suchowski[1,2]

Affiliations.

[1] Condensed Matter Physics Department, School of Physics and Astronomy, Faculty of Exact Sciences, Tel Aviv University, Tel Aviv, 69978, Israel.

[2] Center for Light-Matter Interaction, Tel-Aviv University, Tel-Aviv, 6779801 Israel.

Contact information.

Eyal Bahar* : eyalb@tauex.tau.ac.il

Haim Suchowski: haimsu@tauex.tau.ac.il

Striking a metallic nanostructure with a short and intense pulse of light excites a complex out-of-equilibrium distribution of electrons that rapidly interact and lose their mutual coherent motion. Due to the highly nonlinear dynamics, the photo-excited nanostructures may further emit energetic photons beyond the spectrum of the incident beam, where the shortest pulse duration is traditionally expected to induce the greatest nonlinear emission. Here, we coherently control these photo-induced extreme ultrafast dynamics by spectrally shaping a sub-10 fs pulse within the timescale of coherent plasmon excitations. Contrary to the common perception, we show that stretching the pulse to match its internal phase with the plasmon-resonance increases the second-order nonlinear emission by > 25%. The enhancement is observed only when shaping

extreme-ultrashort pulses (< 20 fs), thus signifying the coherent electronic nature as a crucial source of the effect. We provide a detailed theoretical framework that reveals the optimal pulse shapes for enhanced nonlinear emission regarding the nanostructures' plasmonic-resonances. The demonstrated truly-coherent plasma control paves the way to engineer rapid out-of-equilibrium response in solids state systems and light-harvesting applications.

Coherent control (CC) is an interference-based approach where the phase-correlations of electromagnetic fields are mutually manipulated to steer dynamical processes in matter. It offers many capabilities across scientific disciplines that include control of chemical reactions [1–3], study of biological dynamics [4,5], enhancement of attosecond physics [6], and steering of quantum information processing [7–10]. CC in the optical regime is commonly established by tailoring the temporal shape of a short laser pulse. In the past two decades, the pulse-shaping approach has been extensively used to study and tune the coherent evolution of photo-excited carriers in atomic and molecular systems [1,11–14]. Owing to their long coherence time (hundreds of femtoseconds (fs)), these systems provide comfortable playgrounds to steer the electronic pathways by quantum interference. In turn, CC-induced interference was used to profoundly impact the system's response, including the linear and nonlinear optical emissions [2,3]. In particular, on-demand manipulation and significant enhancement of optical nonlinearities were shown [1,3,13].

On the other hand, many solid-state systems de-cohere very rapidly. Plasmonic nanostructures, which hold the promise to confine, route, and control light at the nanoscale, constitute such a rapidly de-cohering system. In these nanostructures, the manipulation of the geometrical parameters have enabled the observation of extraordinary

linear and nonlinear optical properties [15–19]. Also, the highly-dense radiation initiates complex local dynamics on several time scales (see Figure 1a) [20,21]. Firstly, it excites a collective coherent electronic redistribution (localized plasmons). These de-cohere in 20-30 fs into non-thermal electrons in a highly energetic out-of-equilibrium state. Then, internal collisions among the electrons bring the excited electronic distribution to a fully thermalized state (after few picoseconds). Lastly, relaxation to the lattice temperature is established by *e*-phonon collisions. Substantial observations of the photo-excited ultrafast relaxation evolution has revealed profound phenomena [20,22–24]. In addition, pulse shaping has recently been used, as a further tool to study plasmonic systems [25–31], revealing novel spatio-temporal effects [31–33] as well as utilizing their nonlinear optical response for pulse phase retrieval nonlinear optical generation and nonlinear multicolor imaging [26,29,30,34,35]. However, *true* coherent control of ultrafast plasmon-dynamics requires pulse shaping within the short-lived plasmonic coherent evolution, a challenging task so far due to the metals' dephasing time (~ 20 fs for Gold). Such coherent control, which may allow unprecedented nonlinear optical enhancement in plasmonics systems, as it has in the atomic realm, has however remained elusive.

Here, we demonstrate coherent control of collective electronic dynamics and its direct effect on generated optical nonlinearities. We use sub-10 fs pulse-shaping to match our few-cycle pulse with the internal dynamics of ultrashort plasmonics excitation. We show that, contrary to the common perception, stretching (chirping) the pulse leads to a significant enhancement in the generated second-order optical response exceeding by more than 25% the generation at the maximally compressed ("transform-limited") pulse.

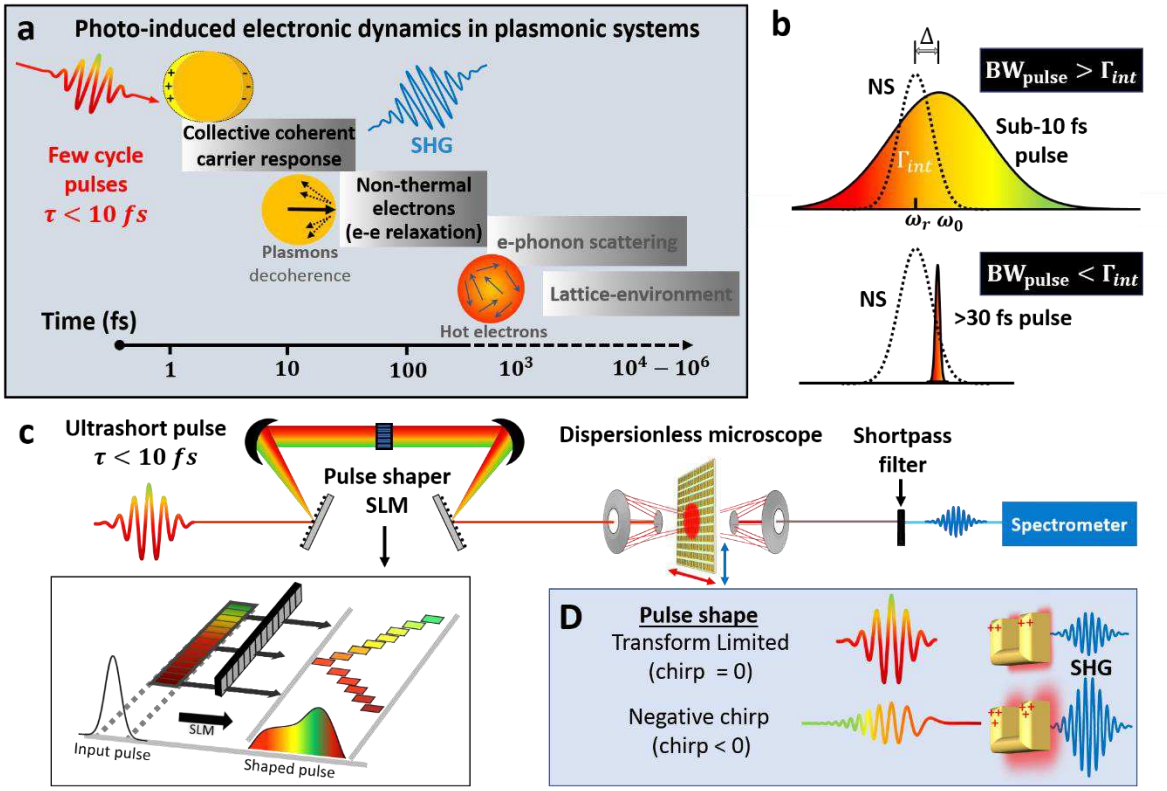

Figure 1 - Coherent control of the photo-induced extreme ultrafast plasmonic excitation. **(a)** The four stages of the photo-excited electronic dynamics (1) collective coherent electronic motion, plasmons, that de-phase in few femtoseconds into a (2) non-thermal electronic state where electron-electron relaxation occurs by the energetic carriers, (3) the electrons become hot and interact with the cold lattice to reach thermal electron-lattice equilibrium, and the (4) lattice-environment equilibration. During carrier excitation, collective electronic multiphoton excitations are induced and can produce second harmonic emission. Out-of-equilibrium dynamics spans up to the third stage. **(b)** The nanostructure's resonance frequency and linewidth, denoted as ω_r and Γ_{int}, can be illuminated by (Upper panel) a sub-10 fs pulse, with much broader than the nanostructure's bandwidth (BW), or (Lower panel) pulse with narrower BW than the nanostructure's linewidth. **(c)** The experimental setup. A sub-10 fs pulse passes through a 4f pulse shaper consisting of a spatial light modulator (SLM, See Inset). The shaped pulses interact with an array of gold nanostructures, producing SHG emission. The mirror-based setup frees the SLM from dispersion management of the pulse and is used only for CC. (**d**) The interaction can be coherently controlled externally by manipulating the pulse's spectral phase to reroute the accumulative excitation-pathways to constructively interfere. A properly induced stretch pulse, despite having a lower intensity than the transform-limited, may lead to a stronger nonlinear plasmonic excitation and produces more SHG emission.

We further measure the second-order generation (SHG) as a function of the chirp parameter and find that the optimal pulse chirp is asymmetrical in time and depends on the nanostructure's geometrical configuration. We devise a theoretical framework that focuses on the dynamics of broad spectral width pulses to efficiently match the broad electronic resonance (figure 1b). The theory suggests that the coherently enhanced nonlinearity stems from the constructive interference of excitation pathways driven by the shaped pulse. We present a direct connection between the optimal pulse durations and the extreme ultrafast

plasmonic decoherence. In particular, the theory allows differentiating between the linearly measured localized Plasmon resonance (LPR)'s linewidth and the intrinsic plasmonic decoherence. Such nonlinear optical enhancement not only provides a clear demonstration for its coherent manipulation but also expands the current understanding of nonlinear plasmonics enhancement, which has been relaying so far on geometrical manipulation of the nanostructures [15–18,23,36].

In our experiments, we use ultrashort pulses with a temporal resolution of sub-10 fs pulse, spanning a bandwidth of more than 300 nm (Venteon Dual, Laser-Quantum, measured linear spectrum in Fig. 2a). The pulses illuminate arrays of U-shaped gold nanostructures, each with different localized plasmon resonance (LPR) (spectral extinction cross-section in Fig. 2a, see supplementary information for more details). Normal incidence second harmonic generation (SHG) was measured for each spectral phase applied to the SLM. In our experiments, the ultrashort pulses' spectral bandwidth exceeds the resonance linewidth of the nanostructures' LPR, (~70 nm Full width-half-max, FWHM). This allows us to simultaneously excite the entire bandwidth of the metallic nanostructure's LPR response, a requirement for coherent control, in addition to enable to reach shorter timescales. This is unlike most previous ultrafast/nonlinear plasmonics experiments that operate with much narrower pulse bandwidths.

We coherently alter the driving pulse shape, using a homemade dispersionless pulse shaper based on spatial light modulator (SLM). The pulse shaper was carefully designed to effectively free the SLM from dispersion management of few-cycle pulses, critically needed for high-fidelity shaping within the plasmonic lifetimes (Supplametary Information). We have verified that the pulse at the illumination plane is maximally compressed in terms of its

linear chirp. Any additional spectral phase applied by the SLM results in a shaped (chirped) pulse with broader temporal width and decreased intensity.

Results:

Figure 2b shows the measured SHG emission from a plasmonic nanostructure with a resonant wavelength of 760 nm as a function of the quadratic spectral phase parameter, ϕ_2 (a.k.a linear chirp). The SHG spectrum induced by the transform-limited pulse ($\phi_2 = 0$) is shown in yellow. Illuminating the nanostructures with positive linear chirp ($\phi_2 = 16fs^2$, blue) results, as expected, in a reduced SHG emission. However, negative linear chirp illumination ($\phi_2 = -16fs^2$, red) shows an increased nonlinear emission of more than 25% in the accumulated SHG compared to the transform-limited pulse. In Figure 2b-II, we introduce a map of the measured SHG emission for a larger range of linear chirp (-150 fs^2 to 150 fs^2 respectively), confirming clear maxima at $\phi_2 = -16fs^2$. Note, the pulse duration spans from sub-10 fs (at $\phi_2 = 0$, maximal pulse peak intensity) to ~155fs at $\phi_2 = \pm 150\ fs^2$(see Supplementary for more Information). Contrary to common perception, in plasmonic nanostructures, the maximal nonlinear generation does not occur when maximizing the peak intensity of the pulse (i.e the shortest pulse).

We compare the results with the SHG signal from a commonly used Beta-Barium-Borate (BBO) nonlinear crystal (See Figure 2d), which has an instantaneous nonlinear response as it is lossless and dispersionless in the near-infrared and optical regime (as dictated by the Kramers–Kronig relations). As expected, in BBO, the maximal SHG is obtained with a transform-limited pulse illumination. We also observe that in distinction to the sign-symmetrical intensity profile found in the BBO crystal, in plasmonic nanostructures, the nonlinear excitation is asymmetrical in relation to the chirp parameter. The asymmetrical

response unravels a coherent structure that dominates the interaction in the first few femtoseconds.

To deepen the understanding of the extreme ultrafast excitation, we study plasmonic nanostructures ranging in their effective lengths, from 130 nm to 300 nm (correspond to

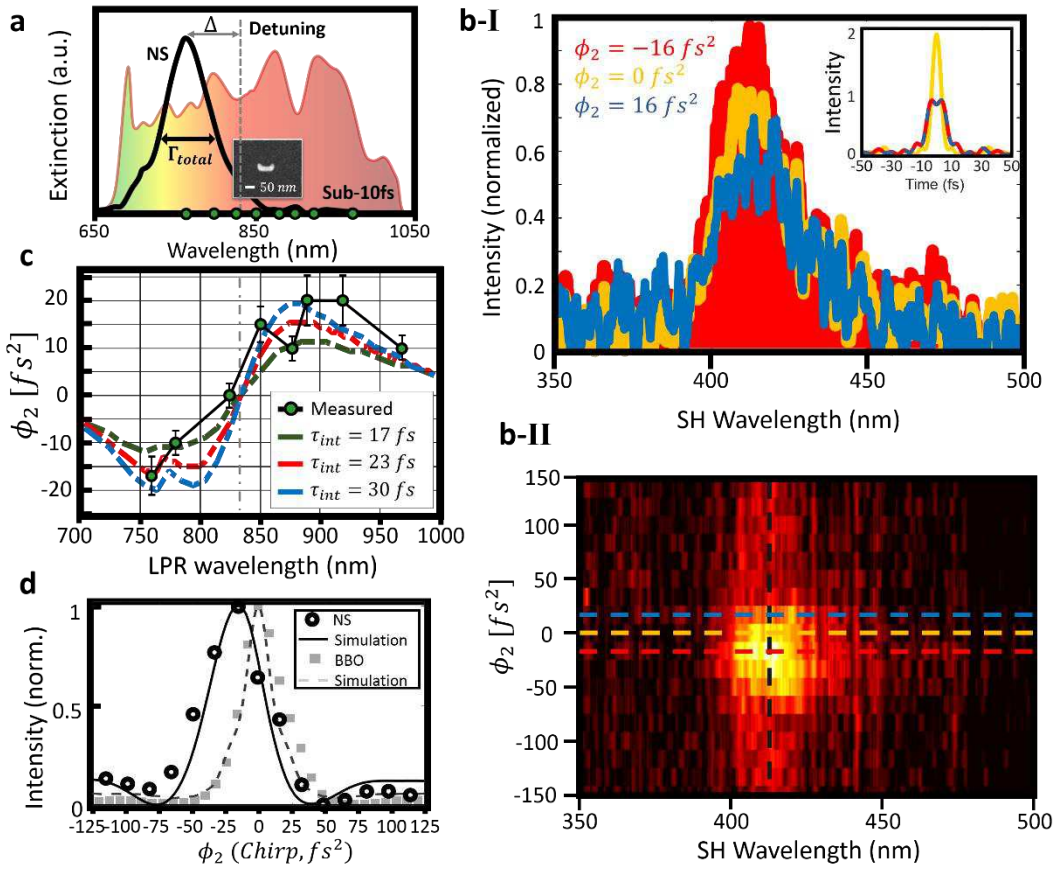

Figure 2 - Enhanced nonlinear second harmonic generation by coherent control (a) Measured laser spectrum (colorful, logarithmic) and measured extinction cross-section of the LPR (black line). Inset: A SEM image of a single nanostructure. **(b-I)** Normalized SHG emission for a positive chirp (dashed blue), unshaped transform-limited pulse (yellow) and negative chirp (red) showing an increase of more than 25% compared to the unshaped pulse and enhanced by 50% compared to the opposite-sign chirped pulse. The inset illustrates the pulses' temporal intensity profiles that is maximal for an unshaped pulse and is equal for both chirp signs. **(b-II)** The SHG emission of plasmonic nanostructure as a function of the linear chirp parameter ϕ_2, controlled via the SLM. In stark contrast to the nonlinear instantaneous interaction, maximal nonlinear emission is obtained $\phi_2 = -16fs^2$, and not at the highest pulse's intensity. The horizontal dashed lines are cross-sections presented in b-I. **(c)** Comparison of SHG emitted by plasmonic nanostructures (circles) and by a BBO crystal (squares) as a function of the chirp parameter. The maximal nonlinear response in plasmonic excitation is negatively shifted due to a non-instantaneous response to the interaction, in contrast to the symmetrically centered instantaneous response measured for a BBO crystal. The experimental results coincide with a numerical simulation based on a 3 level model, our theoretical approach to predict dynamical nonlinear plasmonic excitation. **(d)** Experimental (black dots) measurements of the optimal chirp parameter as a function of the nanostructures resonant wavelengths. Simulation results (dashed) are plotted for several plasmonic decoherence times, τ_{int}. As seen, the simulated value of τ_{int}~$23fs$ best match the experimental results.

LPR's wavelengths 770 nm to 970 nm, respectively). We find a correlation between the optimal linear chirp with the LPR wavelength of the U-shaped nanostructures (See Figure 2d). Importantly, we see that the optimal linear chirp sign is inversely related to detuning, which is defined by the relative location of the plasmonic resonance to the pulse's central wavelength (See Figure 2a). Thus, in positively detuned interactions, where the plasmonic resonant frequency (wavelength) is higher (lower) than the central frequency (wavelength) of the incoming pulse, the optimal linear chirp is negative.

We utilize a theoretical and numerical approach that predicts optical nonlinearities in nanostructures to analyze the evolution of the interaction process capturing the inner dynamics in the multiphoton excitation. In a nutshell, we have considered the interaction as a 3-level *resonant* model solved to the second-order in a time-dependent perturbation framework. The nonlinear polarization reads as follow:

$$\boldsymbol{P}_{\boldsymbol{NL}}^{(\boldsymbol{2})}(\boldsymbol{\Omega}) \propto \sum_{\boldsymbol{\omega}} \boldsymbol{\chi}_{\boldsymbol{eff}}^{(\boldsymbol{2})}(\boldsymbol{\omega},\, \boldsymbol{\omega}_{\boldsymbol{r}},\, \boldsymbol{\Gamma}_{\mathbf{int}})\boldsymbol{E}(\boldsymbol{\omega})\boldsymbol{E}(\boldsymbol{\Omega}-\boldsymbol{\omega}) = \sum_{\boldsymbol{\omega}} \boldsymbol{\chi}^{(\boldsymbol{2})}\boldsymbol{A}(\boldsymbol{\omega})\boldsymbol{A}(\boldsymbol{\Omega}-\boldsymbol{\omega})\frac{\boldsymbol{e}^{\boldsymbol{i}[\boldsymbol{\phi}(\boldsymbol{\omega})+\boldsymbol{\phi}(\boldsymbol{\Omega}-\boldsymbol{\omega})]}}{\boldsymbol{\omega}-\boldsymbol{\omega}_{\boldsymbol{r}}+\boldsymbol{i}\boldsymbol{\Gamma}_{\boldsymbol{int}}}$$

where $\boldsymbol{P}_{\boldsymbol{NL}}^{(\boldsymbol{2})}(\boldsymbol{\Omega})$ is the nonlinear polarization at frequency Ω, $\boldsymbol{E}(\boldsymbol{\omega})$ and $\boldsymbol{E}(\boldsymbol{\Omega}-\boldsymbol{\omega})$ are the linear fields of the fundamental mode, where the generated frequency follows $\Omega = \omega + (\Omega - \omega)$ and $\boldsymbol{\chi}_{\boldsymbol{eff}}^{(\boldsymbol{2})}(\boldsymbol{\omega},\, \boldsymbol{\omega}_{\boldsymbol{r}},\, \boldsymbol{\Gamma}_{\mathbf{int}}) \approx \frac{\chi^{(2)}}{\boldsymbol{\omega}-\boldsymbol{\omega}_{\boldsymbol{r}}+\boldsymbol{i}\boldsymbol{\Gamma}_{\boldsymbol{int}}}$ is the spectral dependent local nonlinear susceptibility that depends on the nanostructures parameters $\boldsymbol{\omega}_{\boldsymbol{r}}$ and $\boldsymbol{\Gamma}_{\mathbf{int}}$. The $\boldsymbol{\chi}^{(\boldsymbol{2})}(\boldsymbol{\omega},\, \boldsymbol{\omega}_{\boldsymbol{r}},\, \boldsymbol{\Gamma}_{\mathbf{int}})$ expands the known geometrical-dependent-only $\boldsymbol{\chi}^{(\boldsymbol{2})}$ term, which results in a generalized nonlinear emission $\boldsymbol{E}_{\boldsymbol{SHG}}(\boldsymbol{\Omega}) \propto \int \boldsymbol{P}_{\boldsymbol{NL}}^{(\boldsymbol{2})}(\boldsymbol{\Omega}) \cdot \boldsymbol{E}(\boldsymbol{\Omega})$ [18]. Our theoretical analysis and observation expand the achievements and great advances in understanding geometry's role in nano-optical nonlinearities generated in singular nanostructures and collective arrays

[15,19,23,38]. The temporal understanding of these resonant nanostructures contributes another dimension to the nonlinear plasmonic analysis and takes it beyond the current state-of-the-art. This process is illustrated schematically in Fig. 3a (See supplementary materials).

From the theory, we find that the nonlinear interaction's coherent structure consists of two contributions: the spectral phase of the ultrafast pulse and the nanostructure's inherent

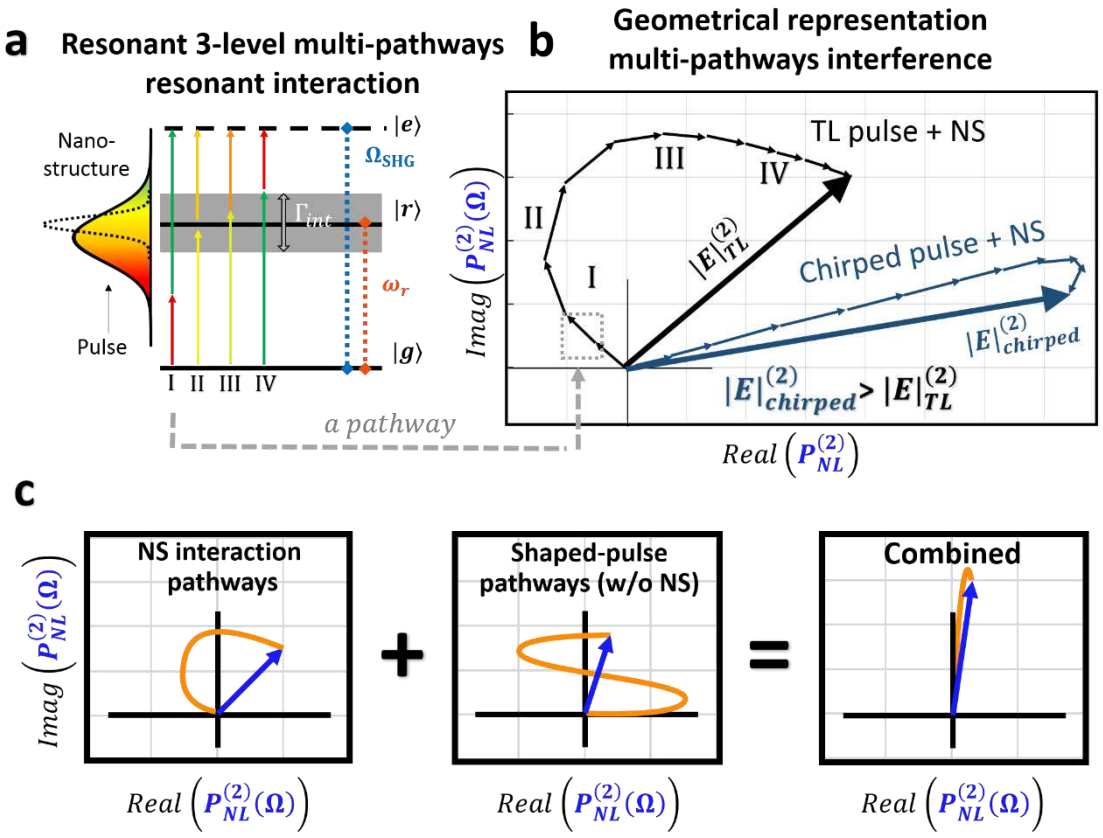

Figure 3 - The plasmonic-mediated second order interaction as the 3-level. (a) An energy level diagram of the pulse-nanostructure interaction. The broadband interaction induces multiple excitation pathways (Feynman paths, four possible pathways are shown) that result in SHG emission. The interference between these interaction pathways can be coherently controlled via spectral pulse shaping. **(b)** Complex valued representation of the Feynman paths of the plasmonic-mediated second-order excitation $P_{NL}^{(2)}$. The broadband interaction induces multiple pathways for excitation (small arrows in the diagram). Each interaction can be represented by the interference of multiple pathways, where the orientation of each arrow stems from the combined phase of both the pulse and nanostructure. The accumulated amplitude, represented by a large arrow, corresponds to the measured intensity of the nonlinear plasmonic excitation. The Feynman diagram of $P_{NL}^{(2)}(\Omega)$ for a maximally compressed pulse, E_{TL} and a chirped pulse, E_{chirp} are illustrated. The chirped pulse enhances the interaction by rerouting the accumulative pathways to constructively interfere. Marked along the trajectory, I-IV, correspond to 4 possible pathways illustrated in Figure 3A. **(c)** The Feynman diagram for the nonlinear ultrafast electronic excitation in the case of (left) a transform limited pulse. (middle) the optimal phase function predicted by the 3-level model without the nanostructures contribution and (right) the combined spectral contribution of both pulse and nanostructure, maximally elongating the amplitude of the interaction according to the 3-level model.

resonant phase. The pulse contribution, controlled at will by the SLM, serves as a probe to study dynamical interactions. The nanostructure's contribution is composed of the amplitude and phase of the spectrally dependent plasmonic response, stemming from the collective electron dynamics, which also incorporate effects of geometry and environment.

To further gain an intuitive physical understanding into the interaction process, we use the pictorial representation in the complex plane along with the numerical simulations. The complex plane representation portrays all spectral components' accumulative contributions in the interaction and is calculated based on a 3-level system approach, as described in detail in the Supplementary information. Our coherent control demonstrations can be intuitively explained by the interfering pathways picture on the complex plane (see Figure 3b). Each excited nonlinear frequency is generated by the coherent accumulation of multiple individual pathways. Each pathway is set by a frequency pair in the driving pulse $\{\omega, \Omega_{SHG} - \omega\}$, dictating $\Omega_{SHG} = \omega + (\Omega_{SHG} - \omega)$. An example for four pathways, set by four frequency pairs, illustrated as paths I to IV.

Inherent to the nanostructures excitation dynamics, the plasmonic response induces self-interfering pathways to the excitation (Figure 3c, left). However, a properly shaped pulse will induce constructive interference between the accumulated pathways, rearranging the trajectory to maximize the nonlinear excitation (Figure 3c, right). Since the unaltered pathways consist of the *intrinsic* destructive interference inherent to the interaction, a reciprocal manipulation to the ultrashort pulse leads to constructive interference in the interaction and to an enhanced excitation *beyond* any other pulse shapes, including the maximally compressed, transform-limited pulse. Our simulations that agree well with the

experimental results provide a complimentary and intuitive understanding for the observed coherently controlled interaction.

Discussion:

We utilize our numerical simulations and compare with the experimental results of the optimal linear chirp for a variety of nanostructures across the spectral landscape. Such simulations offer to separate intrinsic variations in the ultrafast response and to determine the intrinsic lifetime of the coherent excitation, τ_{int}, which is inversely related to the effective interaction linewidth Γ_{int}. We distinguish between the interaction coefficient Γ_{int}, which takes an inherent part in the coherent excitation process, and the total linewidth Γ_{tot}, that represents the steady-state spectral line-width and includes the over-all loss coefficient accessible via incoherent far-field spectral measurements [19]. We make this distinction since the contribution of electronic loss to the coherent collective dynamics in *ultrafast* timescales is yet to be fully understood. It may consist of processes, such as electron-electron scattering, coupling the environment, non-thermalized electron formation and evolution, which are not trivially contributing in the few-femtosecond regime but are captured in the total linewidth measurements. A summary of our simulations is presented in Figure 2d. The optimal chirp parameter is plotted as a function of the nanostructure's LPR for three plasmonic decoherence timescales, 17 fs, 23 fs and 30 fs, commonly used in the literature [19,36]. As seen, the numerical simulations provide very high sensitivity to variations

in decoherence times. Worth noting that in the numerical analysis, the effective interaction linewidth Γ_{int} is the only parameter which is not determined experimentally.

Using our theoretical analysis, which allows predicting the nonlinear excitation leading to SHG for any pulse shape, detuning, and coherence time parameters, we find the *optimal* pulse shape that globally maximizes the nonlinear interaction. More specifically, we find that for plasmonic nanostructures, the optimal spectral phase is $tan^{-1}\left(\frac{\Gamma_{atan}}{\omega-\omega_{atan}}\right)$, where Γ_{atan} and ω_{atan} determine the width and the central frequency of the inverse tangent function, accordingly. Maximal enhancement of SHG for a specific design is obtained when the characteristics of the plasmonic nanostructure set the parameters $\Gamma_{atan} = \Gamma_{NS}$ and $\omega_{atan} = \omega_{NS}$ (see Figure 4). Since the optical nonlinearity is produced separately for each frequency in the manifold of target second harmonic excitations, the optimal pulse shape

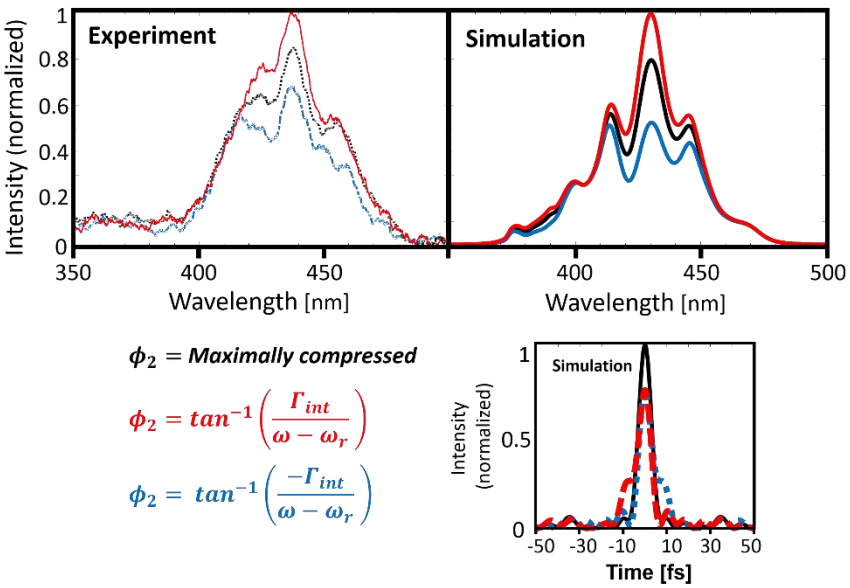

Figure 4 -Optimal nonlinear plasmonic excitation by manipulation the pathways interference. Measured (upper left) and simulated (upper right) SHG induced by the plasmonic excitation for the three pulse shapes: (red) The optimal pulse shape, which is obtained by a spectral phase of an inverse tangent phase function - as predicted by the 3-level model, (black) an unshaped, maximally-compressed pulse, and (blue) an example of differentialy suppressing pulse shape, diminishing the central profile of the generated spectrum while maintaining a constant emission frame. The spectral phase of the inverse tangent function, which is applied by the SLM,can be continuously tunned by changing the value of Γ_{int}, toproduce pulse shapes that vary the generated nonlinear plasmonic excitation spectrum. As dictated by Fourier-transform, the pulse shapes are only slightly deformed in their temporal profiles (lower right) yet have a dramatic effect in the generation of the nonlinear signal.

prediction requires analysis of a range of frequencies (see Supplementary for more Information).

We have verified our predictions experimentally and consistently observe maximal enhancement for the predicted optimal phases. Interestingly, by setting different parameters to the inverse tangent spectral phase, we can uniformly suppress the SHG emission for the central emission profile, maintaining constant profiles of the emission spectra in the generated signal. Taking advantage of this quality, we are able to continuously vary the inverse tangent function to distinctly yet simultaneously facilitate coherent control capabilities in a single-shot. Such control allows contrastingly manipulating to enhance, maintain or suppress specific components in the induced nonlinear spectrum. In order to demonstrate these effects, we selectively manipulate the central spectral profile of the nonlinear emission while effectively maintaining a general form of the emission profile. For example, by setting the parameters to $\omega_{atan} = \omega_{NS}$ and $\Gamma_{atan} = -\Gamma_{int}$, we demonstrate variations in the intensity of up to 200% over the intensity of the SHG emission for particular frequencies while maintaining a constant emission profile for other frequencies. The ability to induce differential control, which is shown to suppress only the central profile of the nonlinear emission, stems from the interference of pathways that correspond to the excited frequency Ω_{SHG}. Therefore, as the interference for each excited nonlinear frequency has a different accumulated composition, the interaction process is effectively manipulated separately for each of the second harmonic frequency components.

To conclude, by ultrafast pulse shaping within the coherence time of the plasmonic evolution's, we unlock fundamental coherent control capabilities and enable the steering and enhancement of the nonlinear optical generation in plasmonic nanostructures. While

coherent excitation in systems with high loss, such as LPRs, are commonly overlooked due to their short-lived, out-of-equilibrium nature, we show that by properly shaping the incoming pulse, the induced excitation can be coherently manipulated throughout the interaction. Notably, such control substantially modifies the nonlinear electronic dynamics with only subtle modifications to the temporal pulse shape and width. Also, the experimental results show that competing processes in the interaction, such as the formation of highly energetic non-thermalized electrons, do not play a significant role in hindering the initial coherence of the plasmonic state. Based on the accumulative interference of the individual spectral components, our theoretical framework is found suitable to explain the experimental results and predict the optimal pulse for maximal global nonlinear enhancement. We believe our coherent control demonstration will promote a paradigm shift in the view of nanoscale nonlinearities, where the origin of optical nonlinearity in nanostructures does not stem only from the enhanced absorption but can rather be dominated by coherent interference.

Furthermore, our fundamental demonstration links the manipulation of photo-excited nanostructure evolution to the vast coherent control schemes explored in atomic and molecular systems. Thus, opening a doorway to implement ultrafast control based on intrinsic plasmonic dynamics is expected to unlock entirely new capabilities desirable in active spatiotemporal metasurfaces at extreme ultrafast speeds [39]. Beyond the significant contribution to fundamental research, we expect that coherent control at extreme ultrafast timescales will provide novel control methods in metamaterials-based applications in nonlinear microscopy, electronic and excitonic dynamics in 2D metamaterials, cancer phototherapy as well as artificial and natural light-harvesting complexes.

Acknowledgments: We thank Dr. Moshe Ben Shalom, Dr. Michael Mrejen, and Dr. Hadar Greener for their valuable input on writing the manuscript, Dr. Inna Shekhtman for her technical support in the fabrication processes of the nanostructures, Dr. Assaf Levanon for his technical support and operation of the laser system. **Funding:** This work was funded by the European Research Council under the grant MIRAGE 20/15 and Israel Science Foundation 1433/15.

Author contributions: EB contributed to the development of the theoretical idea, built the experimental apparatus, conducted the experimental measurements and performed theoretical and data analysis and numerical simulations. MVS performed SEM measurements and analysis. HS conceived the idea and supervised the project. EB and HS prepared the manuscript.

Competing interests: None to declare**.**

Data and materials availability: All data is available in the main text or the supplementary material and any supporting information is available from the author.

References:

1. Brixner, T. & Gerber, G. Quantum control of gas-phase and liquid-phase femtochemistry. *ChemPhysChem* **4**, 418–438 (2003).

2. Shapiro, M. & Brumer, P. *Principles of quantum control of molecular processes*. (Wiley, 2003).

3. Silberberg, Y. Quantum Coherent Control for Nonlinear Spectroscopy and Microscopy. *Annu. Rev. Phys. Chem.* **60**, 277–292 (2009).

4. Wohlleben, W., Buckup, T., Herek, J. L. & Motzkus, M. Coherent Control for Spectroscopy and

Manipulation of Biological Dynamics. *ChemPhysChem* **6**, 850–857 (2005).

5. Rabi, I. I., Zacharias, J. R., Millman, S. & Kusch, P. A new method of measuring nuclear magnetic moment. *Physical Review* **53**, 318 (1938).

6. Katsuki, H., Takei, N., Sommer, C. & Ohmori, K. Ultrafast Coherent Control of Condensed Matter with Attosecond Precision. *Acc. Chem. Res.* **51**, 1174–1184 (2018).

7. Koch, C. P. Controlling open quantum systems: Tools, achievements, and limitations. *Journal of Physics Condensed Matter* **28**, 213001 (2016).

8. Becker, J. N., Görlitz, J., Arend, C., Markham, M. & Becher, C. Ultrafast all-optical coherent control of single silicon vacancy colour centres in diamond. *Nat. Commun.* **7**, 1–6 (2016).

9. Kues, M. *et al.* On-chip generation of high-dimensional entangled quantum states and their coherent control. *Nature* **546**, 622–626 (2017).

10. Shahmoon, E., Levit, S. & Ozeri, R. Qubit coherent control and entanglement with squeezed light fields. *Phys. Rev. A - At. Mol. Opt. Phys.* **80**, 033803 (2009).

11. Koch, C. P., Lemeshko, M. & Sugny, D. Quantum control of molecular rotation. *Rev. Mod. Phys.* **91**, 035005 (2019).

12. Heberle, A. P., Baumberg, J. J. & Köhler, K. Ultrafast coherent control and destruction of excitons in quantum wells. *Phys. Rev. Lett.* **75**, 2598–2601 (1995).

13. Dudovich, N., Dayan, B., Gallagher Faeder, S. M. & Silberberg, Y. Transform-limited pulses are not optimal for resonant multiphoton transitions. *Phys. Rev. Lett.* **86**, 47–50 (2001).

14. Levin, L. *et al.* Coherent control of bond making. *Phys. Rev. Lett.* **114**, 233003 (2015).

15. Kauranen, M. & Zayats, A. V. Nonlinear plasmonics. *Nature Photonics* **6**, 737–748 (2012).

16. Keren-Zur, S., Avayu, O., Michaeli, L. & Ellenbogen, T. Nonlinear Beam Shaping with Plasmonic Metasurfaces. *ACS Photonics* **3**, 117–123 (2016).

17. Ni, X., Emani, N. K., Kildishev, A. V., Boltasseva, A. & Shalaev, V. M. Broadband light bending with plasmonic nanoantennas. *Science* **335**, 427 (2012).

18. O'Brien, K. *et al.* Predicting nonlinear properties of metamaterials from the linear response. *Nat. Mater.* **14**, 379–383 (2015).

19. Cai, W. & Shalaev, V. *Optical metamaterials: Fundamentals and applications*. *Optical Metamaterials: Fundamentals and Applications* (Springer New York, 2010). doi:10.1007/978-1-4419-1151-3

20. Kumar, S. & Sood, A. K. Ultrafast response of plasmonic nanostructures. *arXiv* 131–167 (2018). doi:10.1007/978-3-319-24606-2_6

21. Hartland, G. V. Optical studies of dynamics in noble metal nanostructures. *Chemical Reviews* **111**, 3858–3887 (2011).

22. Stoll, T., Maioli, P., Crut, A., Del Fatti, N. & Vall??e, F. Advances in femto-nano-optics: ultrafast nonlinearity of metal nanoparticles. *Eur. Phys. J. B* **87**, 23–25 (2014).

23. Li, G., Zhang, S. & Zentgraf, T. Nonlinear photonic metasurfaces. *Nature Reviews Materials* **2**, 1–14 (2017).

24. Cho, D.J., Wu, W., Ponizovskaya, E., Chaturvedi, P., Bratkovsky, A.M., Wang, S.Y., Zhang, X., Wang, F. and Shen, Y. . Ultrafast modulation of optical metamaterials. *Opt. Express* **17**, 17652-17657. (2009).

25. Tuchscherer, P. *et al.* Analytic coherent control of plasmon propagation in nanostructures. *Opt. Express* **17**, 14235 (2009).

26. Piatkowski, L., Accanto, N. & Van Hulst, N. F. Ultrafast Meets Ultrasmall: Controlling Nanoantennas and Molecules. *ACS Photonics* **3**, 1401–1414 (2016).

27. Huang, J. S., Voronine, D. V., Tuchscherer, P., Brixner, T. & Hecht, B. Deterministic spatiotemporal control of optical fields in nanoantennas and plasmonic circuits. *Phys. Rev. B* -

Condens. Matter Mater. Phys. **79**, 195441 (2009).

28. Rybka, T. *et al.* Sub-cycle optical phase control of nanotunnelling in the single-electron regime. (2016). doi:10.1038/NPHOTON.2016.174

29. Remesh, V., Stührenberg, M., Saemisch, L., Accanto, N. & Van Hulst, N. F. Phase control of plasmon enhanced two-photon photoluminescence in resonant gold nanoantennas. *Appl. Phys. Lett.* **113**, 211101 (2018).

30. Accanto, N. *et al.* Phase control of femtosecond pulses on the nanoscale using second harmonic nanoparticles. *Light Sci. Appl.* **3**, e143–e143 (2014).

31. Aeschlimann, M. *et al.* Adaptive subwavelength control of nano-optical fields. doi:10.1038/nature05595

32. Brinks, D., Hildner, R., Stefani, F. D. & van Hulst, N. F. Beating spatio-temporal coupling: implications for pulse shaping and coherent control experiments. *Opt. Express* **19**, 26486 (2011).

33. Accanto, N., Piatkowski, L., Renger, J. & Van Hulst, N. F. Capturing the optical phase response of nanoantennas by coherent second-harmonic microscopy. *Nano Lett.* **14**, 4078–4082 (2014).

34. Accanto, N., Piatkowski, L., Hancu, I. M., Renger, J. & Van Hulst, N. F. Resonant plasmonic nanoparticles for multicolor second harmonic imaging. *Appl. Phys. Lett.* **108**, 083115 (2016).

35. Bahar, E., Arieli, U., Mrejen, M. & Suchowski, H. Coherent control of the noninstantaneous nonlinear power-law response in resonant nanostructures. *Phys. Rev. B* **101**, 035141 (2020).

36. Del Fatti, N. & Vallée, F. Ultrafast optical nonlinear properties of metal nanoparticles. *Appl. Phys. B Lasers Opt.* **73**, 383–390 (2001).

37. Materials and methods are available as supplementary materials at the Science website.

38. Michaeli, L., Keren-Zur, S., Avayu, O., Suchowski, H. & Ellenbogen, T. Nonlinear Surface Lattice

Resonance in Plasmonic Nanoparticle Arrays. *Phys. Rev. Lett.* **118**, 243904 (2017).

39. Shaltout, A. M., Shalaev, V. M. & Brongersma, M. L. Spatiotemporal light control with active metasurfaces. *Science* **364**, (2019).

Supplementary Files

This is a list of supplementary files associated with this preprint. Click to download.

- CoherentcontrolultrafastplasmonicsSupp.pdf